

Determination of symmetry energy from experimental and observational constraints; prediction on CREX

Shingo Tagami,¹ Nobutoshi Yasutake,² Mitsunori Fukuda,³ and Masanobu Yahiro^{1,*}

¹*Department of Physics, Kyushu University, Fukuoka 812-8581, Japan*

²*Department of Physics, Chiba Institute of Technology, Chiba 275-0023, Japan*

³*Department of Physics, Osaka University, Osaka 560-0043, Japan*

We determine the symmetry energy $S_{\text{sym}}(\rho)$ at the saturation density $\rho = \rho_0$, particularly for three quantities of $J \equiv S_{\text{sym}}(\rho_0)$, the sloop L , the curvature K_{sym} . The values are evaluated from the observational constraint $M_{\text{max}} \geq 2M_{\text{sun}}$ of neutron star and the experimental constraint on the neutron skin thickness r_{skin}^{208} . The experimental constraint is obtained by taking the weighted mean and its error for three reliable measurements of PREX, electric-dipole polarizability, pygmy strength. One result is $J = 28 - 34$ MeV, $L = 43 - 67$ MeV, $K_{\text{sym}} = (-150) - (-3)$ MeV based on both the observational constraint and the experimental constraint. The other is $J = 27 - 35$ MeV, $L = 43 - 67$ MeV, $K_{\text{sym}} = (-270) - (29)$ MeV based on the experimental constraint only. We also determine the relation between r_{skin}^{48} and r_{skin}^{208} with the correlation coefficient $R = 0.99$. Using the $r_{\text{skin}}^{48} - r_{\text{skin}}^{208}$ relation, we transform the central value of PREX to the corresponding value for r_{skin}^{48} and predict a result of CREX.

I. INTRODUCTION

Many predictions on the symmetry energy $S_{\text{sym}}(\rho)$ have been made so far by taking several experimental and observational constraints on $S_{\text{sym}}(\rho)$ and their combinations. Among the constraints, we take reliable constraints, as show below.

In neutron star (NS), the $S_{\text{sym}}(\rho)$ and its density (ρ) dependence influence strongly the nature within the star. For a pulsar in a binary system, detection of the general relativistic Shapiro delay allows us to determine the mass M of NS. In fact, the NS with $M = 1.97 \pm 0.04M_{\text{sun}}$ is observed [1]. In $\rho = 2 - 3\rho_0$ for the saturation density ρ_0 , the strangeness changing weak decay replaces nucleons by hyperons. The decay makes the maximum mass M_{max} decrease, if the decay occurs really. In this paper, we assume the decay does not take place, because nucleon-hyperon and hyperon-hyperon interactions are still unknown. As an essential constraint on the equation of state (EoS) from astrophysics, we can take

$$M_{\text{max}} \geq 2M_{\text{sun}}. \quad (1)$$

Equation (1) is the most important observational constraint on

$$S_{\text{sym}}(\rho) = J + \frac{L(\rho - \rho_0)}{3\rho_0} + \frac{K_{\text{sym}}(\rho - \rho_0)^2}{18\rho_0^2} + \dots. \quad (2)$$

For the $S_{\text{sym}}(\rho)$, at the present stage, a major aim is to determine $J \equiv S_{\text{sym}}(\rho_0)$, the sloop L and the curvature K_{sym} at $\rho = \rho_0$. The symmetry energy $S_{\text{sym}}(\rho)$ cannot be measured by experiment directly. In place of $S_{\text{sym}}(\rho)$, the neutron-skin thickness r_{skin} is measured to determine L , since a strong correlation between r_{skin}^{208} and L is well known [2, 3]. Meanwhile, for the correlation between

r_{skin}^{208} and J and the correlation between r_{skin}^{208} and K_{sym} , the correlation coefficient R is not shown.

In this paper, we consider reliable experiment constraints on the neutron-skin thickness r_{skin} for double magic nuclei, ^{208}Pb and ^{48}Ca . In this section, we concentrate on ^{208}Pb ; see Sec. II C for ^{48}Ca .

Horowitz, Pollock and Souder proposed a direct measurement for $r_{\text{skin}} = r_{\text{n}} - r_{\text{p}}$ [4]. The measurement is composed of parity-violating and elastic electron scattering; the neutron radius r_{n} is determined from the former experiment, whereas the proton radius r_{p} is from the latter. In fact, for r_{skin}^{208} , the Lead Radius EXperiment (PREX) provides $r_{\text{n}} = 5.78_{-0.18}^{+0.16}$ fm [5, 6]. This result leads to

$$r_{\text{skin}}^{208} = 0.33_{-0.18}^{+0.16} = 0.15 - 0.49 \text{ fm} \quad (3)$$

under $r_{\text{p}}^{208} = 5.45$ fm [7] determined from the elastic electron scattering. Now, the PREX-II and the ^{48}Ca Radius EXperiment (CREX) are ongoing at Jefferson Lab [5]. A result of PREX-II is predicted by taking the central value of the PREX result:

$$r_{\text{skin}}^{208}(\text{PREX II}) = 0.33 \pm 0.06 = 0.27 - 0.39 \text{ fm}; \quad (4)$$

note that 0.06 fm is the estimated error of PREX-II shown in the proposal of CREX [8].

In addition to the direct measurement mentioned above, there are two important indirect measurements for ^{208}Pb . One is measurements of $E1$ polarizability α_{D} and the other is measurements of pygmy dipole resonances. The high-resolution measurement of α_{D} was made for ^{208}Pb in RCNP [9]: The value is

$$r_{\text{skin}}^{208} = 0.156_{-0.021}^{+0.025} = 0.135 - 0.181 \text{ fm}. \quad (5)$$

In this experiment, the value of r_{skin} was measured directly without using the value of r_{p} . The r_{skin}^{208} is also derived from the experimental pygmy strength [10]: The value is

$$r_{\text{skin}}^{208} = 0.24 \pm 0.04 = 0.20 - 0.28 \text{ fm}. \quad (6)$$

* orion093g@gmail.com

We take the weighed mean and its error of the direct and the indirect measured values. The result is

$$r_{\text{skin}}^{208} = 0.18 \pm 0.02 = 0.16 - 0.20 \text{ fm}, \quad (7)$$

This is the most important experimental constraint on r_{skin}^{208} in the present state.

There are many EoSs that show the values of r_{skin}^{208} , J , L , K_{sym} . Chen *et al.* find that existing data on the r_{skin} of Sn isotopes yield an important constraint on L [11]. Combining these constraints with analyses of isospin diffusion and double neutron/proton ratio in heavy-ion collisions at intermediate energies, they predict $L = 58 \pm 18 = 40 - 76$ MeV. Hagen *et al.* calculated a value of r_p for ^{48}Ca , using the coupled-cluster calculation with the chiral interaction. Using the r_p - J and r_p - L correlations, they show $25.2 \lesssim J \lesssim 30.4$ MeV and $37.8 \lesssim L \lesssim 47.7$ MeV [12], where the theoretical errors of J and L mainly come from the systematic uncertainties of the employed Hamiltonians.

In this paper, we determine reliable ranges of J , L and K_{sym} , using the observational constraint (1) and the experimental constraint (7). One set of J , L and K_{sym} is based on both the observational and the experimental constraint, whereas the other set is on the experimental constraint only.

We derive the relation between r_{skin}^{48} and r_{skin}^{208} with the correlation coefficient $R = 0.99$. Using the r_{skin}^{48} - r_{skin}^{208} relation, we transform the central value of PREX to the corresponding values for r_{skin}^{48} and predict a result of CREX, since the proposed error of CREX is smaller than that of PREX-II [8]. We also transform measured values on r_{skin}^{48} to the corresponding results on r_{skin}^{208} . This transformation allows us to compare the transformed data with the original one (7) on r_{skin}^{208} .

We construct two Gogny EoSs, since the number of Gogny EoSs is much smaller than that of Skyrme EoSs.

Section II show our results. Section III is devoted to conclusion.

II. RESULTS

A. Approach to reliable ranges of J , L and K_{sym}

We first accumulate the 204 EoSs from Refs. [3, 11, 13–36] in which r_{skin}^{208} and/or L is presented, since a strong correlation between r_{skin}^{208} and L is shown. In the 204 EoSs of Table I, the number of Gogny EoSs is much smaller than that of Skyrme EoSs. We then construct two EoSs so that D1M* [16] and D1P [22] may become harder; the two EoSs are referred to as D1MK and D1PK, respectively. Eventually, we get the 206 EoSs, as shown in Table I.

For the 206 EoSs, both r_{skin}^{208} and L are obtained self-consistently; the starting r_{skin}^{208} - L relation is determined from the EoSs in which both r_{skin}^{208} and L are presented. The resulting relation

$$L = 620.39 r_{\text{skin}}^{208} - 57.963, \quad (8)$$

has a strong correlation, because of $R = 0.99$. The relation (8) allows us to deduce an empirical constraint on L from the experimental constraint (7). The empirical constraint is

$$L = 41 - 67 \text{ MeV}. \quad (9)$$

In Table I, 47 EoSs satisfy the observational constraint (1). The 47 EoSs are tabulated in Table III. Out of the 47 EoSs, the 23 (D1M*, Sly230a, D2, SLy4, BSk24, BSk21, SFHo, Sly2, SKb, DD-ME2, Sly9, D1PK, DD-ME1, HS(DD2), NL3 $\omega\rho$, APR(E0019), BSk23, SkI6, SkI4, FSUgold2.1, BSR2, SGI, D1AS) satisfy the empirical constraint (9) on L . The 23 yield

$$J = 28 - 34, L = 43 - 67, K_{\text{sym}} = (-150) - (-3) \quad (10)$$

in units of MeV. This is our result based on both the observational constraint (1) and the experimental constraint (7).

In Table I, 95 EoSs satisfy the empirical constraint (9) on L . These are (D1M*, BSk14, SLy230a, M3Y-P6, D2, SLy0, UNEDF0, Ly5, Sk χ m, E0015, SkM*, SLy4, Sly230b, BSk24, D280, BSk21, SV-L47, SFHo, IU-FSU, SLy6, Sly2, SKb, SLy5, SR3, es275, GSkII, SR2, D1P, SII, Ska25-B, SV-sym32-B, DD-ME2, rDD-ME2, M3Y-P7, SV-mas07, SQMC650, SkT3-B, SKRA, Ska35-B, KDE0v1, Sly9, D1PK, DD-ME1, E0024, HA, HS(DD2), SKRA-B, TW99, D1MK, Ducoin, SkT3, NL3 $\omega\rho$, DD, DD-F, SkT1-B, SLy4-B, SkT2, SkT1, SV-sym32, APR, E0019, BSk23, Ska35-T, SkM*-B, SkT2-B, SkT3-T, SV-sym32-T, Ska25-T, SQMC750-B, SQMC700, NRAPR, SkI6, FSUgold, MSL0, SkI4, FSU, FSUgold2.1, rFSUgold, KDE0v1-B, NRAPR-B, NL $\omega\rho$ (025), LNS, BSR2, SkT2-T, SkT1-T, GSkI, Ska25s20, SGI, Ska35s20, SkM*-T, SKRA-T, SkSM*, SLy4-T, BHF-1, D1AS, RAPR). The 95 yield

$$J = 27 - 35, L = 43 - 67, K_{\text{sym}} = (-270) - (29) \quad (11)$$

This is our result based on the experimental constraint (7). The resulting constraint on L is stronger than that of Chen *et al.*.

Further explanation is shown below. We first make three comments on Table I.

1. For D1S, D1N, D1M, D1M*, D1MK, D1P, D1PK, we have calculated r_{skin}^{208} and r_{skin}^{48} with the Hartree-Fock-Bogoliubov method with the angular momentum projection [37]. For the Gogny EoSs, the effective nucleon-nucleon interaction can be described as

$$\begin{aligned} V(\vec{r}) = & \sum_{i=1,2} t_0^i (1 + x_0^i P_\sigma) \rho^{\alpha_i} \delta(\vec{r}) \\ & + \sum_{i=1,2} (W_i + B_i P_\sigma - H_i P_\tau - M_i P_\sigma P_\tau) e^{-\frac{r^2}{\mu_i^2}} \\ & + iW_0(\sigma_1 + \sigma_2)[\vec{k}' \times \delta(\vec{r})\vec{k}], \end{aligned} \quad (12)$$

where σ and τ are the Pauli spin and isospin operators, respectively, and the corresponding exchange operators P_σ and P_τ are defined as usual. See Table II for the parameter sets of D1MK and D1PK. As shown in Table I, the results of D1MK and D1PK for r_{skin}^{208} and r_{skin}^{48} are consistent with the experimental constraint (7) on r_{skin}^{208} and the experimental constraint (15) on r_{skin}^{48} . For matter, the energy density functional has been used.

2. Dutra *et al.* proposed a series of criteria derived from macroscopic properties of nuclear matter in the vicinity of nuclear saturation density derived by the liquid drop model, experiments with giant resonances and heavy-ion collisions, and selected 16 EoSs from 240 Skyrme EoSs by using a series of criteria [29]. The 16 EoSs (GSkI, GSkII, KDE0v1, LNS, MSL0, NRAPR, Ska25s20, Ska35s20, SKRA, SkT1, SkT2, SkT3, Skxs20, SQMC650, SQMC700, SV-sym32) are in Table I.
3. Out of the 240 Skyrme EoSs, Tsang *et al.* selected 12 EoSs (KDE0v1, NRAPR, Ska25, Ska35, SKRA, SkT1, SkT2, SkT3, SQMC750, SV-sym32, SLY4, SkM*) and fitted them to nuclear binding energies, charge radii and single-particle energies [14]. The fitted set is identified with the label “-T” from the original set. Brown and Schwenk fitted the original set so that the effective mass m^*/m can be 0.9 in neutron matter at $\rho = 0.10 \text{ fm}^{-3}$ [30]. This set is identified with the label by “-B”. The three sets are in Table I.

Figure 1 shows r_{skin}^{208} dependence of J , L , K , K_{sym} for 206 EoSs of Table I, where K and K_{sym} are the incompressibility and the symmetry-energy incompressibility, respectively. The dotted lines denote Eq. (8) for the r_{skin}^{208} - L and

$$J = 48.287 r_{\text{skin}}^{208} + 23.091. \quad (13)$$

for the r_{skin}^{208} - J relation. The r_{skin}^{208} - L relation ($R = 0.99$) is much stronger than the r_{skin}^{208} - J relation ($R = 0.74$), the r_{skin}^{208} - K relation ($R = 0.30$), and the r_{skin}^{208} - K_{sym} relation ($R = 0.84$).

The M - R relation of NS is shown in Fig. 2 for D1MK and D1PK, where R is a radius of NS. In our calculations, the beta-equilibrium is taken into account. Below the subnuclear density $n < 0.1 \text{ fm}^{-3}$, we use the BPS EoS [38]. D1PK satisfies the observable constraint (1). Meanwhile, the maximum mass $M_{\text{max}} = 1.94M_{\text{sun}}$ of D1MK is slightly smaller than the observable constraint (1), but is in the $M = 1.97 \pm 0.04M_{\text{sun}}$ of Ref. [1]

Horowitz mentioned some observational constraints and the lower limit of R determined from PREX [39]; his mention is illustrated in Fig. 2. Bauswein *et al.* suggested that if $1.6 M_{\text{sun}}$ stars have radii less than the indicated lower limit, the NS in GW170817 would collapse to soon to a black hole and not eject material enough to power

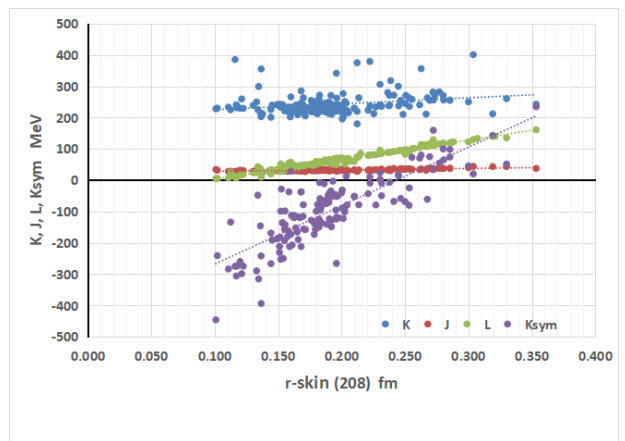


FIG. 1. Properties of 206 EoSs (dotted) as a function of r_{skin}^{208} . The dotted lines stand for Eq. (8) for the r_{skin}^{208} - L and Eq. (13) for the r_{skin}^{208} - J .

the observed Kilonova. When the maximum mass of a NS is above the red dotted line, Metzger *et al.* argued that the compact remnant in GW170817 lives too long and provides too much energy to the kilonova. Finally the GW170817 limit on the radius of a $1.4M_{\text{sun}}$ is from the limit on the gravitational deformability, whereas the limit on the EoS at low density from PREX is plotted as a minimum radius of a $0.5M_{\text{sun}}$ NS. Such low mass NSs have low central densities comparable to nuclear density. As an interesting result, D1PK satisfies all of the observation constraints mentioned above and the lower bound of R determined from PREX. D1MK almost satisfies the observation constraints mentioned above and the lower bound of R determined from PREX.

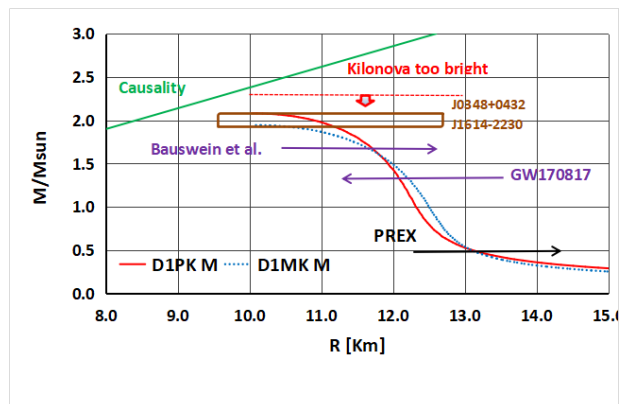


FIG. 2. M - R relation for D1MK and D1PK. D1PK is shown by the solid line, and D1MK is by the dashed line. See the text for the observation constraints shown and the lower limit of R determined from PREX.

B. Relation between r_{skin}^{48} and r_{skin}^{208}

For the 206 EoSs in Table I, we determine the relation between r_{skin}^{208} and r_{skin}^{48} self-consistently, where the

starting r_{skin}^{208} - r_{skin}^{48} relation is determined from the EoSs in which both r_{skin}^{208} and r_{skin}^{48} are presented. The result reads

$$r_{\text{skin}}^{48} = 0.5547 r_{\text{skin}}^{208} + 0.0718; \quad (14)$$

see Fig. 3. The correlation is quite strong, because of $R = 0.99$.

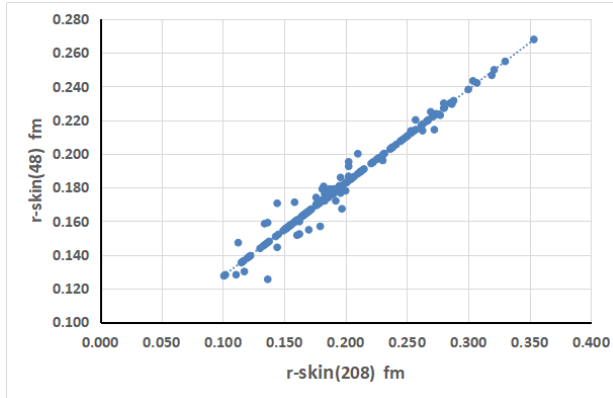


FIG. 3. Relation between r_{skin}^{208} and r_{skin}^{48} . The dotted line stands for Eq. (14), while dots correspond to 206 EoSs. Two vertical lines denote the experimental constraint (7) on r_{skin}^{208} , while two horizontal lines correspond to the experimental constraint (15) on r_{skin}^{48} .

C. Prediction of CREX

The high-resolution measurement of α_D was applied for ^{48}Ca in RCNP [40]: The value is

$$r_{\text{skin}}^{48} = 0.17 \pm 0.03 = 0.14 - 0.20 \text{ fm}. \quad (15)$$

Very lately, Tanaka *et al.* have determined

$$r_{\text{skin}}^{48} = 0.146 \pm 0.048 \text{ fm} \quad (16)$$

by measuring interaction cross sections for ^{48}Ca scattering on a C target in RIKEN [41]. Before the measurement of Ref. [41], we predicted the interaction cross section and the r_{skin}^{48} , using D1S [42]. The predicted value $r_{\text{skin}}^{48} = 0.159$ fm is in Eq. (16), and the predicted interaction cross section agrees with the measured one..

The data (16) has almost the same accuracy as the high-resolution measurement Eq. (15). We then calculate the weighed mean and its error of Eq. (15) and Eq (16): The result is

$$r_{\text{skin}}^{48} = 0.16 \pm 0.03 = 0.13 - 0.19 \text{ fm}. \quad (17)$$

This is the most important constraint on r_{skin}^{48} at the present stage. The coupled-cluster result $0.12 \lesssim r_{\text{skin}}^{48} \lesssim 0.15$ fm with the chiral interaction [12] is consistent with the experimental constraint (17).

In the proposal of CREX [8], the estimated error is 0.02 fm. Using Eq. (14), we transform the central value 0.33 fm of PREX to the corresponding value

$r_{\text{skin}}^{48} = 0.47$ fm. Therefore, we may predict a result of CREX as

$$r_{\text{skin}}^{48}(\text{CREX}) = 0.47 \pm 0.02 = 0.45 - 0.49 \text{ fm}. \quad (18)$$

This is too large in comparison with the present indirect result (17). This implies that the central value is large. We predict a CREX result by taking the central value of Eq. (17). This ia

$$r_{\text{skin}}^{48} = 0.16 \pm 0.02 = 0.14 - 0.18 \text{ fm}; \quad (19)$$

note that 0.02 fm is the estimated error of CREX [8].

D. Comparison between data r_{skin}^{48} and data r_{skin}^{208}

Applying the r_{skin}^{208} - r_{skin}^{48} relation (14) for the experimental constraint (17) on r_{skin}^{48} , we can get

$$r_{\text{skin}}^{208} = 0.15 - 0.18 \text{ fm}. \quad (20)$$

The indirect range (20) is slightly smaller than the original one (7) on r_{skin}^{208} . We then take the weighted mean and its error from the original and indirect ranges: The result is

$$r_{\text{skin}}^{208} = 0.18 \pm 0.02 = 0.16 - 0.20 \text{ fm}. \quad (21)$$

The final result (21) agrees with the original one (7) including PREX.

III. CONCLUSION

We have determined two reliable ranges of J , L and K_{sym} by taking the observational constraint (1) and the experimental constraint (7). One is $J = 28 - 34$ MeV, $L = 43 - 67$ MeV, $K_{\text{sym}} = (-150) - (-3)$ MeV of Eq. (10) based on both the observational constraint (1) and the experimental constraint (7). The other is $J = 27 - 35$ MeV, $L = 43 - 67$ MeV, $K_{\text{sym}} = (-270) - (29)$ MeV of Eq. (11) based on the experimental constraint (7) only.

In addition, we have determined the r_{skin}^{208} - r_{skin}^{48} relation (14) with the correlation coefficient $R = 0.99$. In the proposal of CREX, the estimated error 0.02 fm of CREX is smaller than 0.06 fm of PREX-II. We then transform the central value $r_{\text{skin}}^{208} = 0.33$ fm of PREX to the corresponding value $r_{\text{skin}}^{48} = 0.47$ fm, using the the relation (14). We get $r_{\text{skin}}^{48} = 0.47 \pm 0.02 = 0.45 - 0.49$ fm as a prediction of CREX. However, it is too large compared with the range (17) measured for r_{skin}^{48} . Taking the central value 0.16 fm of the range (17), we predict a result of CREX as $r_{\text{skin}}^{48}(\text{CREX}) = 0.16 \pm 0.02 = 0.14 - 0.18$ fm of Eq. (19).

In the 204EoSs of Table I, the number of Gogny EoSs is much smaller than that of Skyrme EoSs. We have then constructed two Gogny EoSs, D1MK and D1PK. As for J , L , K_{sym} , the values of D1MK and D1PK are in the reliable range of Eq (10). For r_{skin}^{208} and r_{skin}^{48} , the values of D1MK and D1PK are consistent with the experimental

constraints (7) and (17). D1PK satisfies all of the observational constraint Eq. (1), the experimental constraint (7) on r_{skin}^{208} , and the experimental constraints Eq. (17)

ACKNOWLEDGEMENTS

Yahiro thanks Dr. M. Toyokawa heartily. The authors express our gratitude to Dr. Y. R. Shimizu for his useful information.

-
- [1] P. Demorest, T. Pennucci, S. Ransom, M. Roberts and J. Hessels, *Nature* **467**, 1081 (2010), [arXiv:1010.5788 [astro-ph.HE]].
- [2] B. A. Brown, *Phys. Rev. Lett.* **111**, no. 23, 232502 (2013), [arXiv:1308.3664 [nucl-th]].
- [3] X. Roca-Maza, M. Centelles, X. Vinas and M. Warda, *Phys. Rev. Lett.* **106**, 252501 (2011), [arXiv:1103.1762 [nucl-th]].
- [4] C. J. Horowitz, S. J. Pollock, P. A. Souder and R. Michaels, *Phys. Rev. C* **63**, 025501 (2001), [nucl-th/9912038].
- [5] R. Michaels *et al.*, Lead Radius Experiment PREX proposal 2005; <http://halloweb.jlab.org/parity/prex/>.
- [6] S. Abrahamyan *et al.*, *Phys. Rev. Lett.* **108**, 112502 (2012), [arXiv:1201.2568 [nucl-ex]].
- [7] A. Ong, J. C. Berengut and V. V. Flambaum, *Phys. Rev. C* **82**, 014320 (2010), [arXiv:1006.5508 [nucl-th]].
- [8] The CREX proposal is available in the homepage “halloweb.jlab.org/parity/prex”.
- [9] A. Tamii *et al.*, *Phys. Rev. Lett.* **107**, 062502 (2011).
- [10] A. Klimkiewicz *et al.*, *Phys. Rev. C* **76**, 051603 (2007).
- [11] L. W. Chen, C. M. Ko, B. A. Li and J. Xu, *Phys. Rev. C* **82**, 024321 (2010), [arXiv:1004.4672 [nucl-th]].
- [12] G. Hagen *et al.*, *Nature Phys.* **12**, no. 2, 186 (2015), [arXiv:1509.07169 [nucl-th]].
- [13] A. Akmal, V. R. Pandharipande and D. G. Ravenhall, *Phys. Rev. C* **58**, 1804 (1998), [nucl-th/9804027].
- [14] C. Y. Tsang, B. A. Brown, F. J. Fattoyev, W. G. Lynch and M. B. Tsang, *Phys. Rev. C* **100**, no. 6, 062801 (2019), [arXiv:1908.11842 [nucl-th]].
- [15] C. Ishizuka, T. Suda, H. Suzuki, A. Ohnishi, K. Sumiyoshi and H. Toki, *Publ. Astron. Soc. Jap.* **67**, 13 (2015), [arXiv:1408.6230 [nucl-th]].
- [16] C. Gonzalez-Boquera, M. Centelles, X. Vinas and L. M. Robledo, *Phys. Lett. B* **779**, 195 (2018), [arXiv:1712.06735 [nucl-th]].
- [17] M. Farine, D. Von-Eiff, P. Schuck, J. F. Berger, J. Decharge, and M. Girod, *J. Phys. G* **25**, 863 (1999).
- [18] C. Gonzalez-Boquera, M. Centelles, X. Vinas and A. Rios, *Phys. Rev. C* **96**, no. 6, 065806 (2017), [arXiv:1706.02736 [nucl-th]].
- [19] M. Oertel, M. Hempel, T. Klähn and S. Typel, *Rev. Mod. Phys.* **89**, no. 1, 015007 (2017), [arXiv:1610.03361 [astro-ph.HE]].
- [20] J. Piekarewicz, *Phys. Rev. C* **76**, 064310 (2007), [arXiv:0709.2699 [nucl-th]].
- [21] Y. Lim, K. Kwak, C. H. Hyun and C. H. Lee, *Phys. Rev. C* **89**, no. 5, 055804 (2014), [arXiv:1312.2640 [nucl-th]].
- [22] R. Sellahewa and A. Rios, *Phys. Rev. C* **90**, no. 5, 054327 (2014), [arXiv:1407.8138 [nucl-th]].
- [23] T. Inakura and H. Nakada, *Phys. Rev. C* **92**, 064302 (2015), [arXiv:1509.02982 [nucl-th]].
- [24] F. J. Fattoyev and J. Piekarewicz, *Phys. Rev. Lett.* **111**, 162501 (2013), [arXiv:1306.6034 [nucl-th]].
- [25] A. W. Steiner, M. Prakash, J. M. Lattimer and P. J. Ellis, *Phys. Rept.* **411**, 325 (2005), [nucl-th/0410066].
- [26] M. Centelles, X. Roca-Maza, X. Vinas and M. Warda, *Phys. Rev. C* **82**, 054314 (2010), [arXiv:1010.5396 [nucl-th]].
- [27] C. Ducoin, J. Margueron and C. Providencia, *EPL* **91**, no. 3, 32001 (2010), [arXiv:1004.5197 [nucl-th]].
- [28] M. Fortin, C. Providencia, A. R. Raduta, F. Gulminelli, J. L. Zdunik, P. Haensel and M. Bejger, *Phys. Rev. C* **94**, no. 3, 035804 (2016), [arXiv:1604.01944 [astro-ph.SR]].
- [29] M. Dutra, O. Lourenco, J. S. Sa Martins, A. Delfino, J. R. Stone and P. D. Stevenson, *Phys. Rev. C* **85**, 035201 (2012), [arXiv:1202.3902 [nucl-th]].
- [30] B. A. Brown and A. Schwenk, *Phys. Rev. C* **89**, no. 1, 011307 (2014), Erratum: [*Phys. Rev. C* **91**, no. 4, 049902 (2015)]. [arXiv:1311.3957 [nucl-th]].
- [31] B. A. Brown, *Phys. Rev. Lett.* **85**, 5296 (2000).
- [32] P.-G. Reinhard, A. S. Umar, P. D. Stevenson, J. Piekarewicz, V. E. Oberacker and J. A. Maruhn, *Phys. Rev. C* **93**, no. 4, 044618 (2016), [arXiv:1603.01319 [nucl-th]].
- [33] Z. Zhang, Y. Lim, J. W. Holt and C. M. Ko, *Phys. Lett. B* **777**, 73 (2018) doi:10.1016/j.physletb.2017.12.012 [arXiv:1703.00866 [nucl-th]].
- [34] P. W. Zhao and S. Gandolfi, *Phys. Rev. C* **94**, no. 4, 041302 (2016), [arXiv:1604.01490 [nucl-th]].
- [35] Y. Wang, C. Guo, Q. Li, H. Zhang, Y. Leifels and W. Trautmann, *Phys. Rev. C* **89**, no. 4, 044603 (2014) doi:10.1103/PhysRevC.89.044603 [arXiv:1403.7041 [nucl-th]].
- [36] O. Lourenco, M. Bhuyan, C. H. Lenzi, M. Dutra, C. Gonzalez-Boquera, M. Centelles and X. Vinas, arXiv:2002.06242 [nucl-th].
- [37] S. Tagami, Y. R. Shimizu and J. Dudek, *Phys. Rev. C* **87**, 054306 (2013), [arXiv:1301.3279 [nucl-th]].
- [38] G. Baym, C. Pethick and P. Sutherland, *Astrophys. J.* **170**, 299 (1971).
- [39] C. J. Horowitz, *Annals Phys.* **411**, 167992 (2019), [arXiv:1911.00411 [astro-ph.HE]].
- [40] J. Birkhan *et al.*, *Phys. Rev. Lett.* **118**, no. 25, 252501 (2017), [arXiv:1611.07072 [nucl-ex]].
- [41] M. Tanaka *et al.*, to be published in *Phys. Rev. Lett.* arXiv:1911.05262 [nucl-ex].
- [42] S. Tagami, M. Tanaka, M. Takechi, M. Fukuda and M. Yahiro, *Phys. Rev. C* **101**, no. 1, 014620 (2020), [arXiv:1911.05417 [nucl-th]].
- [43] J. Yang, J. A. Hernandez and J. Piekarewicz, *Phys. Rev. C* **100**, no. 5, 054301 (2019), [arXiv:1908.10939 [nucl-th]].

TABLE I. Properties of 206 EoSs (1). The symbol \ddagger is our results, while \dagger denotes the results of self-consistent calculations.

	m*/m	K	J	L	Ksym	Rskin-208	Rskin-48	Refs.
APR, E0019		266.000	32.600	57.600		0.160	0.160 [†]	[13, 15, 31]
BHF-1		195.500	34.300	66.550	-31.300	0.200 [†]	0.183 [†]	[27]
BSk14	0.800	239.380	30.000	43.910	-152.030	0.164 [†]	0.162 [†]	[27, 29]
BSk16	0.800	241.730	30.000	34.870	-187.390	0.149 [†]	0.154 [†]	[27, 29]
BSk17	0.800	241.740	30.000	36.280	-181.860	0.151 [†]	0.156 [†]	[27, 29]
BSk20	0.800	241.400	30.000	37.400	-136.500	0.153 [†]	0.157 [†]	[28, 29]
BSk21	0.800	245.800	30.000	46.600	-37.200	0.168 [†]	0.165 [†]	[28, 29]
BSk22		245.900	32.000	68.500	13.000	0.204 [†]	0.185 [†]	[28]
BSk23		245.700	31.000	57.800	-11.300	0.186 [†]	0.175 [†]	[15, 28]
BSk24		245.500	30.000	46.400	-37.600	0.168 [†]	0.165 [†]	[28]
BSk25		236.000	29.000	36.900	-28.500	0.152 [†]	0.156 [†]	[28]
BSk26		240.800	30.000	37.500	-135.600	0.153 [†]	0.157 [†]	[28]
BSR2		239.900	31.500	62.000	-3.100	0.193 [†]	0.179 [†]	[28]
BSR6		235.800	35.600	85.700	-49.600	0.231 [†]	0.200 [†]	[28]
D1		229.400	30.700	18.360	-274.600	0.122 [†]	0.139 [†]	[18]
D1AS		229.400	31.300	66.550	-89.100	0.200 [†]	0.183 [†]	[18]
D1M	0.746 [‡]	224.958 [‡]	28.552 [‡]	24.966 [‡]	-133.692 [‡]	0.113 [‡]	0.147 [‡]	[16]
D1M*	0.746 [‡]	225.365 [‡]	30.249 [‡]	43.311 [‡]	-47.793 [‡]	0.134 [‡]	0.158 [‡]	[16]
D1MK	0.746 [‡]	225.400 [‡]	33.000 [‡]	55.000 [‡]	-37.275 [‡]	0.158 [‡]	0.171 [‡]	TW
D1N	0.748 [‡]	225.525 [‡]	29.594 [‡]	33.665 [‡]	-168.750 [‡]	0.144 [‡]	0.171 [‡]	[16]
D1P	0.672 [‡]	250.860 [‡]	32.418 [‡]	49.827 [‡]	-157.419 [‡]	0.179 [‡]	0.157 [‡]	[17, 18]
D1PK	0.700 [‡]	260.000 [‡]	33.000 [‡]	55.000 [‡]	-150.000 [‡]	0.182 [‡]	0.181 [‡]	TW
D1S	0.697 [‡]	202.856 [‡]	31.125 [‡]	22.558 [‡]	-241.797 [‡]	0.137 [‡]	0.159 [‡]	[16, 23]
D2	0.738	209.300	31.130	44.850		0.165 [†]	0.163 [†]	[16]
D250		249.900	31.570	24.820	-289.400	0.133 [†]	0.145 [†]	[18]
D260		259.500	30.110	17.570	-298.700	0.121 [†]	0.139 [†]	[18]
D280		285.200	33.140	46.530	-211.900	0.168 [†]	0.165 [†]	[18]
D300		299.100	31.220	25.840	-315.100	0.135 [†]	0.146 [†]	[18]
DD		241.000	31.700	56.000	-95.000	0.183 [†]	0.173 [†]	[11]
DD-F		223.000	31.600	56.000	-140.000	0.183 [†]	0.173 [†]	[11]
DD-ME1		245.000	33.100	55.000	-101.000	0.203 [†]	0.193 [†]	[11, 15, 27, 34]
DD-ME2		251.000	32.300	51.240	-87.000	0.203 [†]	0.187 [†]	[11, 27, 28, 34]
DD-PC1				67.799		0.203 [†]	0.195 [†]	[27, 34]
Ducoin		240.200	32.760	55.300	-124.700	0.182 [†]	0.173 [†]	[27, 34]
E0008(TMA)		318.000	30.660	90.140		0.239 [†]	0.204 [†]	[15]
E0009		280.000	32.500	88.700		0.236 [†]	0.203 [†]	[15, 19]
E0015		216.700	30.030	45.780		0.167	0.164	[15]
E0024		244.500	33.100	55.000		0.182 [†]	0.172	[15]
E0025		211.000	31.600	107.400		0.267 [†]	0.220 [†]	[15]
E0036		281.000	36.900	110.800		0.272 [†]	0.223 [†]	[15]
es25		211.730	25.000	27.749 [†]		0.138	0.148 [†]	[25]
es275		205.330	27.500	48.549 [†]		0.171	0.167 [†]	[25, 28]
es30		215.360	30.000	69.603 [†]		0.205	0.186 [†]	[25]
es325		212.450	32.500	81.925 [†]		0.225	0.197 [†]	[25]
es35		209.970	34.937	96.182 [†]		0.248	0.210 [†]	[25]
FKVW		379.000	33.100	80.000	11.000	0.222 [†]	0.195 [†]	[11]
FSU		230.000	32.590	60.500	-51.300	0.210	0.188 [†]	[24, 27]
FSUgold		229.000	32.500	60.000	-52.000	0.210	0.200	[11, 19, 20]
FSUgold2.1		230.000	32.590	60.500		0.191 [†]	0.177 [†]	[15, 19]
GM1		299.700	32.480	93.870	17.890	0.245 [†]	0.207 [†]	[27, 28]
GM3		239.900	32.480	89.660	-6.470	0.238 [†]	0.204 [†]	[27]
Gs		237.570	31.384	89.304 [†]		0.237	0.203 [†]	[25]
GSkI		230.210	32.030	63.450	-95.290	0.195 [†]	0.180 [†]	[29]
GSkII	0.790	233.400	30.490	48.630	-157.830	0.171 [†]	0.167 [†]	[29]
GT2		228.100	33.940	5.020	-445.900	0.101 [†]	0.127 [†]	[18]
G σ		237.290	31.370	94.020	13.990	0.245 [†]	0.208 [†]	[27]
HA		233.000	30.700	55.000	-135.000	0.182 [†]	0.172 [†]	[11]
HFB-17				36.300		0.151	0.155 [†]	[3]
HFB-8				14.800		0.115	0.135 [†]	[3]
HS(DD2)		243.000	31.700	55.000	-93.200	0.182 [†]	0.172 [†]	[19, 28]
IU-FSU		231.200	31.300	47.200	28.700	0.160	0.160 [†]	[19, 24]
KDE0v1	0.740	227.540	34.580	54.690	-127.120	0.181 [†]	0.172 [†]	[29]
KDE0v1-B	0.790	216.000	34.900	61.000		0.192	0.172	[30]
KDE0v1-T	0.810	217.000	34.600	72.000	-40.000	0.200	0.178	[14]

TABLE I. Properties of 206 EoSs (2).

	m*/m	K	J	L	Ksym	Rskin-208	Rskin-48	Refs.
LNS	0.830	210.780	33.430	61.450	-127.360	0.192 [†]	0.178 [†]	[27, 29]
LS180		180.000	28.600	73.800		0.212 [†]	0.189 [†]	[15, 19, 29]
LS220		220.000	28.600	73.800		0.212 [†]	0.189 [†]	[15, 19, 29]
LS375		375.000	28.600	73.800		0.212 [†]	0.189 [†]	[15, 19, 29]
Ly5		229.940	32.010	45.243 [†]		0.166	0.164 [†]	[25]
M3Y-P6		239.700	32.100	44.600	-165.300	0.165 [†]	0.163 [†]	[21, 23]
M3Y-P7		254.700	31.700	51.500	-127.800	0.176 [†]	0.169 [†]	[23, 28]
MSk3	1.000	233.250	28.000	7.040	-283.520	0.111	0.128	[29, 34]
MSk6	1.050	231.170	28.000	9.630	-274.330	0.118	0.130	[29, 34]
MSk7	1.050	385.360	27.950	9.400	-274.630	0.116	0.136 [†]	[3, 29]
MSL0	0.800	230.000	30.000	60.000	-99.330	0.180	0.171 [†]	[11, 29, 35]
NL1		212.000	43.500	140.000	143.000	0.319	0.247	[11, 34]
NL2		401.000	44.000	130.000	20.000	0.304	0.243	[11, 34]
NL3		271.000	37.300	118.000	100.000	0.280	0.230	[11, 20, 24, 26–28]
NL3*				119.769 [†]		0.287	0.230	[34]
NL3 $\omega\rho$		271.600	31.700	55.500	-7.600	0.183 [†]	0.173 [†]	[28]
NL4		270.350	36.239	111.649 [†]		0.273	0.223 [†]	[25]
NL-SH		356.000	36.100	114.000	80.000	0.263	0.214	[11, 34]
NL ρ		240.000	30.300	85.000	3.000	0.230 [†]	0.199 [†]	[11]
NL $\omega\rho$ (025)		270.700	32.350	61.050	-34.360	0.192 [†]	0.178 [†]	[27]
NRAPR	0.690	225.700	32.787	59.630	-123.320	0.190	0.177 [†]	[25, 29]
NRAPR-B	0.850	225.000	35.100	61.000		0.193	0.178	[30]
NRAPR-T	0.730	221.000	34.100	70.000	-46.000	0.195	0.181	[14]
PC-F1		255.000	37.800	117.000	75.000	0.269	0.225	[11, 34]
PC-F2		256.000	37.600	116.000	65.000	0.281 [†]	0.227 [†]	[11, 34, 35]
PC-F3		256.000	38.300	119.000	74.000	0.285 [†]	0.230 [†]	[11, 34]
PC-F4		255.000	37.700	119.000	98.000	0.285 [†]	0.230 [†]	[11]
PC-LA		263.000	37.200	108.000	-61.000	0.268 [†]	0.220 [†]	[11]
PC-PK1				101.478		0.257	0.220	[34]
PK1		282.000	37.600	116.000	55.000	0.277	0.223	[11, 34]
PKDD		263.000	36.900	90.000	-80.000	0.253	0.214	[11, 34]
RAPR		276.700	33.987	66.958 [†]		0.201	0.183 [†]	[25]
RATP		239.580	29.260	32.390	-191.250	0.145 [†]	0.152 [†]	[27]
rDD-ME2				51.300		0.193	0.179 [†]	[3]
rFSUGold				60.500		0.207	0.186 [†]	[3, 28]
rG2				100.700		0.257	0.214 [†]	[3]
rNL1				140.100		0.321	0.250 [†]	[3]
rNL3				118.500		0.280	0.227 [†]	[3]
rNL3*				122.600		0.288	0.232 [†]	[3]
rNLC				108.000		0.263	0.218 [†]	[3]
rNL-RA1				115.400		0.274	0.224 [†]	[3]
rNL-SH				113.600		0.266	0.219 [†]	[3]
rNL-Z				133.300		0.307	0.242 [†]	[3]
Rs		237.660	30.593	80.096 [†]	-9.100	0.222	0.195 [†]	[25, 28]
rTM1				110.800		0.271	0.222 [†]	[3]
R σ		237.410	30.580	85.700	-9.130	0.231 [†]	0.200 [†]	[27]
S271		271.000	35.927	97.541 [†]		0.251	0.211 [†]	[25]
SFH \circ		245.000	31.600	47.100		0.169 [†]	0.165 [†]	[19]
SFHx		239.000	28.700	23.200		0.130 [†]	0.144 [†]	[19]
SGI	0.610	262.000	28.300	63.900	-51.990	0.196 [†]	0.180 [†]	[21, 25, 29]
SGII	0.790	214.700	26.830	37.620	-145.920	0.136	0.147 [†]	[3, 23, 27, 29]
SII	0.580	341.400	34.160	50.020	-265.720	0.196	0.177	[34]
SIII	0.760	355.37	28.160	9.910	-393.730	0.137	0.125	[29, 34]
Sk χ m		230.400	30.940	45.600		0.167	0.164 [†]	[29, 33]
SK255		254.960	37.400	95.000	-58.300	0.247 [†]	0.208 [†]	[28]
SK272		271.550	37.400	91.700	-67.800	0.241 [†]	0.205 [†]	[28]
Ska	0.610	263.160	32.910	74.620	-78.460	0.214 [†]	0.190 [†]	[3, 19, 23, 28, 29, 35]
Ska25-B	0.990	219.000	32.500	51.000		0.176	0.170	[30]
Ska25s20	0.980	220.750	33.780	63.810	-118.220	0.196 [†]	0.180 [†]	[29]
Ska25-T	0.980	220.000	31.900	59.000	-59.000	0.183	0.176	[14]
Ska35-B	1.000	244.000	32.800	54.000		0.180	0.172	[30]
Ska35s20	1.000	240.270	33.570	64.830	-120.320	0.198 [†]	0.181 [†]	[29, 35]
Ska35-T	0.990	238.000	32.000	58.000	-84.000	0.184	0.177	[14, 27, 29]

TABLE I. Properties of 206 EoSs (3).

	m*/m	K	J	L	Ksym	Rskin-208	Rskin-48	Refs.
SKb	0.610	263.000	33.880	47.600	-78.500	0.170 [†]	0.166 [†]	[28, 29]
SkI1	0.690	242.750	37.530	161.050	234.670	0.353 [†]	0.268 [†]	[29, 35]
SkI2	0.680	240.700	33.400	104.300	70.600	0.262 [†]	0.217 [†]	[23, 27–29]
SkI3	0.580	258.000	34.800	100.500	72.900	0.255 [†]	0.213 [†]	[23, 27–29]
SkI4	0.650	247.700	29.500	60.400	-40.600	0.191 [†]	0.177 [†]	[21, 23, 27–29]
SkI5	0.580	255.800	36.697	129.300	159.500	0.272	0.214	[23, 25, 27–29]
SkI6	0.640	248.650	30.090	59.700	-47.270	0.189 [†]	0.177 [†]	[27–29]
SkM*	0.790	216.610	30.030	45.780	-155.940	0.170	0.155	[3, 23, 29, 34]
SkM*-B	0.780	218.000	34.200	58.000		0.187	0.175	[30]
SkM*-T	0.790	219.000	33.700	65.000	-65.000	0.187	0.179	[14?]
SkMP	0.650	230.930	29.890	70.310	-49.820	0.197	0.167	[3, 27? , 28]
SkO	0.900	223.390	31.970	79.140	-43.170	0.221 [†]	0.194 [†]	[27, 29]
SKOp	0.900	222.360	31.950	68.940	-78.820	0.204 [†]	0.185 [†]	[28, 29]
SKP	1.000	200.970	30.000	19.680	-266.600	0.144	0.144	[29, 34]
SKRA	0.750	216.980	31.320	53.040	-139.280	0.179 [†]	0.171 [†]	[29]
SKRA-B	0.790	212.000	33.700	55.000		0.181	0.172	[29, 30]
SKRA-T	0.800	213.000	33.400	65.000	-55.000	0.190	0.179	[14, 29]
Sk-Rs				85.700		0.215	0.191 [†]	[3]
SkSM*				65.500		0.197	0.181 [†]	[3]
SkT1	1.000	236.160	32.020	56.180	-134.830	0.184 [†]	0.173 [†]	[29]
SkT1-B	0.970	242.000	33.300	56.000		0.183	0.172	[30]
SkT1-T	0.970	238.000	32.600	63.000	-70.000	0.190	0.179	[14, 29]
SkT2	1.000	235.730	32.000	56.160	-134.670	0.184 [†]	0.173 [†]	[29]
SkT2-B	0.970	242.000	33.500	58.000		0.186	0.174	[30]
SkT2-T	0.960	238.000	32.600	62.000	-75.000	0.188	0.178	[14, 29]
SkT3	1.000	235.740	31.500	55.310	-132.050	0.182 [†]	0.173 [†]	[29]
SkT3-B	0.980	241.000	32.700	53.000		0.179	0.172	[30]
SkT3-T	0.970	236.000	31.900	58.000	-80.000	0.183	0.178	[14]
Sk-T4	1.000	235.560	35.457	94.100	-24.500	0.253	0.212 [†]	[3, 23, 25]
Sk-T6	1.000	235.950	29.970	30.900	-211.530	0.151	0.155 [†]	[3, 29]
Skxs20	0.960	201.950	35.500	67.060	-122.310	0.201 [†]	0.183 [†]	[29]
Skz2	0.700	230.070	32.010	16.810	-259.660	0.120 [†]	0.138 [†]	[29, 35]
Skz4	0.700	230.080	32.010	5.750	-240.860	0.102 [†]	0.128 [†]	[29, 35]
SLy0	0.700	229.670	31.982	44.873 [†]	-116.230	0.165	0.163 [†]	[25, 29]
SLy10	0.680	229.740	31.980	38.740	-142.190	0.155 [†]	0.158 [†]	[27, 29]
Sly2	0.700	229.920	32.000	47.460	-115.130	0.170 [†]	0.166 [†]	[28, 29]
SLy230a	0.700	229.890	31.980	44.310	-98.210	0.155	0.158 [†]	[25, 27–29]
Sly230b	0.690	229.960	32.010	45.960	-119.720	0.167 [†]	0.164 [†]	[27, 29]
SLy4	0.690	229.900	32.000	45.900	-119.700	0.162	0.152	[3, 16, 21, 23, 28, 34]
SLy4-B	0.700	224.000	34.100	56.000		0.184	0.174	[30]
SLy4-T	0.760	222.000	33.600	66.000	-55.000	0.191	0.179	[14, 29]
SLy5	0.700	229.920	32.010	48.150	-112.760	0.162	0.160	[29, 34]
SLy6	0.690	229.860	31.960	47.450	-112.710	0.161	0.152	[29, 34]
Sly9	0.670	229.840	31.980	54.860	-81.420	0.182 [†]	0.172 [†]	[28, 29]
SQMC650	0.780	218.110	33.650	52.920	-173.150	0.178 [†]	0.171 [†]	[29]
SQMC700	0.760	222.200	33.470	59.060	-140.840	0.188 [†]	0.176 [†]	[29]
SQMC750-B	0.710	228.000	34.800	59.000		0.190	0.176	[30]
SQMC750-T	0.750	223.000	33.900	68.000	-50.000	0.194	0.180	[14, 29]
SR1	0.900	202.150	29.000	41.245 [†]		0.160	0.160 [†]	[25]
SR2		224.640	30.071	49.130 [†]		0.172	0.167 [†]	[25]
SR3		222.550	29.001	48.308 [†]		0.171	0.166 [†]	[25]
SV	0.380	306.000	32.800	96.100	24.190	0.230	0.196	[21, 27, 29, 34]
SV-bas	0.900	221.760	30.000	32.000	-156.570	0.155	0.158 [†]	[29, 32]
SV-K218	0.900	218.230	30.000	35.000	-206.870	0.161	0.161 [†]	[29, 32]
SV-K226	0.900	225.820	30.000	34.000	-211.920	0.159	0.160 [†]	[29, 32]
SV-K241	0.900	241.070	30.000	31.000	-230.770	0.151	0.155 [†]	[29, 32]
SV-kap00	0.900	233.440	30.000	40.000	-161.780	0.158	0.159 [†]	[29, 32]
SV-kap20	0.900	233.440	30.000	36.000	-193.190	0.155	0.158 [†]	[29, 32]
SV-kap60	0.900	233.450	30.000	29.000	-249.750	0.154	0.157 [†]	[29, 32]
SV-L25	0.900		30.000	25.000		0.143	0.151 [†]	[32]
SV-L32	0.900		30.000	32.000		0.154	0.157 [†]	[32]
SV-L40	0.900	233.3	30.000	40.000		0.166	0.164 [†]	[32]
SV-L47	0.900	233.4	30.000	47.000		0.177	0.170 [†]	[32]

TABLE I. Properties of 206 EoSs (4).

	m*/m	K	J	L	Ksym	Rskin-208	Rskin-48	Refs.
SV-mas07	0.700	233.540	30.000	52.000	-98.770	0.152	0.156 [†]	[29, 32]
SV-mas08	0.800	233.130	30.000	40.000	-172.380	0.160	0.160 [†]	[29, 32, 35]
SV-mas10	1.000	234.330	30.000	28.000	-252.500	0.152	0.156 [†]	[29, 32]
SV-sym28	0.900	240.860	28.000	7.000	-305.940	0.117	0.136 [†]	[29, 32]
SV-sym32	0.900	233.810	32.000	57.000	-148.790	0.192	0.178 [†]	[29, 32]
SV-sym32-B	0.910	237.000	32.300	51.000		0.176	0.174	[30]
SV-sym32-T	0.910	232.000	31.500	58.000	-77.000	0.181	0.179	[14]
SV-sym34	0.900	234.070	34.000	81.000	-79.080	0.227	0.198 [†]	[29, 32, 35]
TFa		245.100	35.050	82.500	-68.400	0.250	0.210 [†]	[24]
TFb		250.100	40.070	122.500	45.800	0.300	0.238 [†]	[24]
TFc		260.500	43.670	135.200	51.600	0.330	0.255 [†]	[24]
TM1		281.000	36.900	110.800	33.550	0.272 [†]	0.223 [†]	[11, 15, 27, 28]
TW99		241.000	32.800	55.000	-124.000	0.196	0.186	[11, 34]
UNEDF0		229.800	30.500	45.100	-189.600	0.166 [†]	0.164 [†]	[23, 29]
UNEDF1		219.800	29.000	40.000	-179.400	0.158 [†]	0.159 [†]	[23]
Z271		271.000	35.369	89.520 [†]		0.238	0.204 [†]	[25]

TABLE II. Parameter sets of D1MK and D1PK.

D1MK	μ_i	W_i	B_i	H_i	M_i	t_0^i	x_0^i	α_i	W_0
$i = 1$	0.5	-17242.0144	19604.4056	-20699.9856	16408.6002	1561.7167	1	1/3	115.36
$i = 2$	1.0	642.607965	-941.150253	865.572486	-845.300794	0	-1	1	
D1PK	μ_i	W_i	B_i	H_i	M_i	t_0^i	x_0^i	α_i	W_0
$i = 1$	0.90	-465.027582	155.134492	-506.775323	117.749903	981.065351	1	1/3	130
$i = 2$	1.44	34.6200000	-14.0800000	70.9500000	-41.3518104	534.155654	-1	1	

TABLE III. Properties of 47 EoSs satisfying the observational constraint.

	J	L	Ksym	R-max	M-max	Refs.
APR, E0019	32.60	57.60		10.0	2.20	[13, 15, 31]
BSk20	30.00	37.40	-136.50	10.2	2.17	[28, 29]
BSk21	30.00	46.60	-37.20	11.0	2.29	[28, 29]
BSk22	32.00	68.50	13.00	11.2	2.27	[28]
BSk23	31.00	57.80	-11.30	11.2	2.28	[15, 28]
BSk24	30.00	46.40	-37.60	11.2	2.29	[28]
BSk25	29.00	36.90	-28.50	11.2	2.23	[28]
BSk26	30.00	37.50	-135.60	10.2	2.18	[28]
BSR2	31.50	62.00	-3.10	11.9	2.38	[28]
BSR6	35.60	85.70	-49.60	12.1	2.44	[28]
D1AS	31.30	66.55	-89.10	10.0	2.00	[18]
D1M*	30.25	43.15	-47.79	9.6	2.00	[16, 36]
D1PK	33.00	55.00	-150.00	10.0	2.1	TW
D2	31.13	44.85		10.2	2.1	[16, 36]
DD-ME1	33.10	55.00		11.9	2.47	[11, 15, 27, 34]
DD-ME2	32.30	51.20	-87.00	12.2	2.48	[11, 27, 28, 34]
E0008(TMA)	30.66	90.14		12.4	2.04	[15]
FSUgold2.1	32.60	60.50		12.1	2.13	[15, 19]
GM1	32.50	94.40	17.89	12.0	2.36	[27, 28]
HS(DD2)	31.70	55.00	-93.20	11.8	2.42	[19, 28]
LS220	28.60	73.80		10.6	2.05	[15, 19, 29]
LS375	28.60	73.80		12.6	2.72	[15, 19, 29]
NL3	37.30	118.00	100.00	13.3	2.77	[11, 20, 24, 26-28]
NL3 $\omega\rho$	31.70	55.50	-7.60	13.0	2.75	[28]
Rs	30.59	80.06	-9.10	10.8	2.12	[25, 28]
SFHo	31.60	47.10		10.5	2.05	[19]
SFHx	28.70	23.20		10.9	2.14	[19]
SGI	28.30	63.90	-51.99	12.0	2.25	[21, 25, 28, 29]
SK255	37.40	95.00	-58.30	11.0	2.15	[28]
SK272	37.40	91.70	-67.80	11.2	2.24	[28]
SKa	32.91	74.62	-78.46	11.0	2.21	[3, 19, 23, 28, 29, 35]
SKb	33.88	47.60	-78.50	10.6	2.2	[28, 29]
SkI2	33.40	104.30	70.60	11.3	2.17	[23, 27-29]
SkI3	34.80	100.50	72.90	11.4	2.25	[23, 27-29]
SkI4	29.50	60.40	-40.60	10.6	2.18	[21, 23, 27-29]
SKI5	36.70	129.30	159.50	11.3	2.25	[23, 25, 27-29]
SkI6	30.09	59.70	-47.27	11.2	2.2	[23, 25, 27-29]
SkMP	29.89	70.31	-49.82	10.8	2.11	[3, 27? , 28]
Sly2	32.00	47.46	-115.13	10.0	2.06	[28, 29]
Sly230a	31.98	44.31	-98.21	10.3	2.11	[25, 27-29]
SLy4	32.00	45.90	-119.70	10.0	2.06	[3, 16, 21, 23, 28, 34]
Sly9	31.98	54.86	-81.42	10.6	2.16	[28, 29]
SV	32.80	96.10		11.7	2.44	[21, 27, 29, 34]
TFa	35.05	82.50		12.2	2.10	[24]
TFb	40.07	122.50		12.6	2.15	[24]
TFc	43.67	135.20		12.9	2.21	[24]
TM1	36.90	110.80		12.5	2.18	[11, 15, 27, 28]